Catalysis Today 443 (2025) 114965

Contents lists available at ScienceDirect

Catalysis Today

journal homepage: www.elsevier.com/locate/cattod

Mixed metal oxide bronzes as catalysts for the gas-phase aerobic transformation of glycerol to acrylic acid: Single or double catalytic bed approaches

Agustín de Arriba [*], Daniel Delgado [1], Patricia Concepción, José M. López Nieto [*]

Instituto de Tecnología Química, Universitat Politecnica de Valencia-Consejo Superior de Investigaciones Científicas, Avenida de los Naranjos s/n, Valencia 46022, Spain

ARTICLE INFO

Keywords:
HTB tungsten oxides
Mo-V-O M1 catalysts
Oxydehydration of glycerol
Acrylic acid

ABSTRACT

Metal-doped hexagonal tungsten oxide bronzes (*h*-WVO_x and *h*-$WNbO_x$) and metal-doped orthorhombic molybdenum oxide bronzes-M1 type ($MoVO_x$, $MoVTeO_x$ and $MoVTeNbO_x$) have been synthesized hydrothermally and heat-treated at 400, 550 or 600 °C in N_2. The catalysts were characterized by several techniques and tested in the one-pot aerobic transformation of glycerol at 350 °C. From all of them, *h*-$WNbO_x$ resulted as the most selective to acrolein (80 % yield), whereas both *h*-WVO_x and $MoVTeNbO_x$ were more effective to acrylic acid (with a yield lower than 25 %). Subsequently, a double-bed reactor comparative study was conducted, with *h*-$WNbO_x$ acting as the first catalytic bed. In this case, the yield to acrylic acid decreased as follows: $MoVTeNbO_x$ > $MoVTeO_x$ > $MoVO_x$ > *h*-WVO_x. IR spectroscopy of acrolein adsorbed on these catalysts allows to explain the catalytic performance of these catalysts.

1. Introduction

Acrylic acid (AA) is one of the most important chemical intermediates for the production of many industrial and consumer products [1]. The market volume of acrylic acid worldwide amounted to nearly 8.12 million metric tons (in 2022), and it is forecast that will grow to around 11.9 million metric tons in 2030. [2].

AA is currently produced primarily through a commercial, two-stage propylene-based process, using both two different catalysts and two reaction conditions [3]. In this case, an overall acrylic acid selectivity of 85–90 % (propene-based) is achieved with propene conversions above 95 % [3]. However, it has been estimated that 175 kg of CO_2 are produced for every ton of propylene processed [4]. Due to the increasing cost of propylene and the environmental impact, alternative feedstocks such as propane and biomass-derived compounds have been studied in the last years.

From propane, the best catalytic results have been obtained by partial oxidation over multicomponent catalysts based on Mo-V-Nb-Te(Sb)-O (so-called M1 phase) in a single step [5–8]. In this case, the reaction is carried out by the first formation of propylene on V-O-Mo sites, which is then adsorbed on other active sites (i.e., Te-O-Mo pairs) for the formation of acrylic acid. Regretfully, this process is kinetically limited to a maximum of 50 % yield to acrylic acid, and this is due to the intrinsic lower selectivity and stability of the acrylic acid when compared to the two-step industrial process from propylene [9].

In the current context, both the increasing emissions of carbon dioxides and the increase in the price of petroleum resources urges the development of technologies using renewable feedstocks. In this way, renewable resources have been also proposed as feedstocks for the synthesis of olefins, intermediates (acrylates, etc.) or sustainable polymers [10,11]. Therefore, it has been proposed the synthesis of acrylic acid by the selective transformation of bio-sources including glycerol, lactic acid, 3-hydroxipropanoic acid or acetic acid [12–18].

In the case of single step reactions, a wide range of heterogenous materials such as: heteropolyacids [19], zeolitic materials [20], Mo-V-based catalysts [21–24] and W-based metal oxide bronzes (including hexagonal W-V-O [25], W-V-Nb-O [26] and $PO_4/W_{2.2}V_{0.4}Nb_{2.4}O_{14}$ [27]), in addition to amorphous tungsten-incorporated molybdenum vanadium mixed oxide (MoVWO) [28] and a pseudocrystalline W-Mo-V-O [29], have been proposed as active and selective catalysts in one-pot aerobic transformation of glycerol to acrylic acid. Nevertheless, as observed for the selective transformation of propane to acrylic acid, the interaction of acrylic acid with the acid sites of the different catalysts studied also limits its yield to

* Corresponding authors.
E-mail addresses: agdear@itq.upv.es (A. de Arriba), jmlopez@itq.upv.es (J.M. López Nieto).
[1] Present address: Department of Inorganic Chemistry, Fritz-Haber-Institut der Max-Planck-Gesellschaft, Faradayweg 4–6, Berlin, 14195, Germany

https://doi.org/10.1016/j.cattod.2024.114965
Received 15 May 2024; Received in revised form 5 July 2024; Accepted 28 July 2024
Available online 29 July 2024

no more than 50 %.

On the other hand, the use of two different catalytic beds has been proposed more recently. Thus, in the two-catalyst approach, yields of acrylic acid up to 70 % can be achieved by using first a Zr/W/O acid catalyst for glycerol dehydration and then a Cu/Sr-doped W/V/Mo/O system for acrolein oxidation [30], however, these results were obtained by employing two subsequent separated reactors.

Conversely, AA can be also produced in a single reactor via successive oxidation of the dehydrated glycerol in separated sequential beds using both zeolitic materials and mixed metal oxides. In this sense, by combining HZSM-5 and V-Mo mixed oxides supported on silicic acid, a 40 % yield to acrylic acid can be achieved [31]. Moreover, by modifying the second catalytic bed with W-doped MoVO, AA yield can be increased up to ca. 47.2 % at 250 °C (whereas W-doped MoVO in single bed only reports ca. 30 % acrylic acid yield) [32]. On the contrary, replacing the first zeolitic bed for $H_4SiW_{12}O_{40}/Al_2O_3$, maintaining Mo_3VO_x as second bed catalyst, results in decreased acrylic acid yields, lower than 30 %, although no changes were observed when the catalysts were physically mixed [33].

Finally, enhanced catalytic results in double bed configuration were obtained by Liu *et al.* employing a $Cs_{2.5}H_{0.5}PW_{12}O_{40}$ catalyst supported on Nb_2O_5 as the first catalytic bed (yield to acrolein of 79.5 %), and a V-Mo oxide supported on SiC as the second catalytic bed, with yields to acrylic acid up to ca. 75 %, also widely outperforming results in single bed configuration (only 25 % acrylic acid yield) [34].

Herein, we report the use of a two catalytic bed configuration system as an effective method for the direct conversion of glycerol to acrylic in aerobic conditions. In this way, in a first bed, a W-Nb-O metal oxide bronze with hexagonal tungsten bronze structure (HTB) initially transforms glycerol into acrolein by acid catalysis. Then, in a second bed, M1-type catalysts with different chemical compositions (i.e., Mo-V-O, Mo-V-Te-O or Mo-V-Te-Nb-O) were studied in order to selectively transform acrolein to acrylic acid by partial oxidation reaction. To facilitate the discussion on the importance of the composition of M1-based catalysts in the final selectivity to acrylic acid, an *in situ* IR spectroscopy study is also presented using the adsorption of the reaction intermediate (i.e., acrolein), which can help to identify the nature of active and selective sites in the oxidation catalysts.

2. Experimental

2.1. Catalyst preparation

The two different families of catalysts (i.e., W-based and M1-based) were prepared by two similar hydrothermal methods already reported in the literature.

In this sense, W-M-O mixed oxides (M= V or Nb) with hexagonal tungsten bronze (HTB) structure, and with molar ratios in the synthesis gels of W/V= 1.0/0.3 and W/Nb = 1.0/0.2, were synthesized hydrothermally from aqueous solutions of the metallic precursors, namely: ammonium metatungstate, vanadyl sulfate and/or ammonium niobate (V) oxalate hydrate [26]. Synthesis gels were transferred to Teflon-lined stainless-steel autoclaves and heated at 175 °C for 48 h. Finally, solids were thermally activated at 550 °C for 2 h under N_2 stream and named as ***h*-WNbO** or ***h*-WVO**. For comparison, pure hexagonal tungsten bronze, ***h*-WO_x** sample, was also prepared hydrothermally [26], and then activated at 400 °C for 2 h under N_2 stream.

On the other hand, M1-based catalysts, Mo-V-(Te)-(Nb)-O mixed oxides were prepared hydrothermally, from aqueous solutions of ammonium heptamolybdate, vanadyl sulfate, telluric acid/tellurium dioxide and ammonium niobate(V) oxalate hydrate, as previously reported [35], using the following composition (and pH) in the synthesis gel: Mo/V/Te/Nb= 1/0.25/0.17/0.17 (synthesized at pH= 2.2), Mo/V/Te= 1/0.37/0.17 (at pH= 2.2) or Mo/V= 1/0.37 (at pH= 3.0). The corresponding solids were heat-treated at 600 °C (Mo/V/Te/Nb and Mo/V/Te) or 400 °C (Mo/V) during 2 h in a N_2 stream. The catalysts will be named as **MoVTeNbO**, **MoVTeO** and **MoVO**, respectively.

2.2. Catalyst characterization

The specific surface areas were determined from N_2 adsorption isotherms at −190 °C, using the BET method, in a Micromeritics ASAP 2000 instrument. Samples were previously degassed under vacuum at 250 °C before adsorption.

Powder X-ray diffraction patterns (XRD) were collected using a Panalytical XPert diffractometer equipped with a graphite monochromator operating at 40 kV and 30 mA, employing Ni-filtered CuKα radiation (λ= 0.1542 nm).

X-ray photoelectron spectroscopy (XPS) analyses were performed on a SPECS spectrometer equipped with a Phoibos 150 MCD-9 detector, employing a monochromatic X-ray source (Al Kα, 1486.6 eV). An operating pressure of 10^{-9} mbar, along with an X-ray power of 100 W and an analyzer pass of 30 eV were used. Data treatment was performed using CASA XPS software, referring binding energies to C *1 s* at 284.5 eV in all cases.

Ammonia temperature programmed desorption (TPD-NH_3) experiments were performed in a Micromeritics TPD/2900 equipment. In a typical experimental measurement, samples (ca. 50 mg) were heated at 300 °C for 1 h under argon flow to be subsequently cooled down to 100 °C and saturated with ammonia. Then, solids were kept under inert gas flow (100 °C / 15 minutes) to eliminate physically adsorbed NH_3. TPD analyses were carried out in the 100–600 °C temperature range (heating rate of 10 °C min^{-1}) with desorbed ammonia being analyzed by both mass spectroscopy and a thermal conductivity detector (TCD) analyzer.

The crystal morphology was studied by Scanning Electron Microscopy (SEM) in a JEOL 6300 Microscope, working at a voltage of 2 kV, and average chemical composition was determined by energy-dispersive X-ray spectroscopy (XEDS), with an acquisition time for each spectrum of 120 s, by using an Oxford LINK ISIS detector attached to the microscope. Measures took place at the Microscopy Service of the Polytechnic University of Valencia (UPV).

Temperature-programmed reduction (TPR-H_2) experiments took place in a Micromeritics Autochem 2910 devise, equipped with a TCD detector. Composition of the reducing gas consisted of 10 % H_2 diluted in argon, and a total flow rate of 50 mL min^{-1}. Catalysts were treated until 600 or 800 °C, depending on the composition, at a heating rate of 10 °C min^{-1}.

IR spectroscopy studies of adsorbed acrolein were performed in a Bruker Vertex 70 spectrometer using a DTGS detector and acquired at 4 cm^{-1} resolutions. A homemade IR cell for *in situ* treatments was connected to a vacuum system with a gas dosing facility allowing to vary both atmosphere and temperature (from 25 to 500 °C). For every experiment, an activation at 200 °C for 90 min under O_2 was considered. After that, samples were cooled down to 150 °C and kept under vacuum conditions for 1 h, subsequently recording several spectra while cooling down to room temperature. Once samples are at room temperature, ca. 3 mbar of acrolein and 6 mbar of O_2 were dosed to the cell and then it was closed. Temperature was increased at 100, 150, 200 and 250 °C, maintaining each temperature for 30 min. IR spectra were recorded after each temperature on the “hot” and “cooled down” pellet to favor the adsorption of products desorbed to the gas phase.

2.3. Catalytic tests

The gas phase aerobic transformation of glycerol (Gly, $\mathbf{C_3H_8O_3}$) was initially carried out in one-pot, in a fixed-bed reactor (quartz made, 11 mm inner diameter), in the temperature range 300–400 °C, at atmospheric pressure, with a feed composition of $Gly/O_2/H_2O/He$= 2/4/40/54 molar ratio, and a contact time, W/F, of 80 g_{CAT} h $(mol_{Gly})^{-1}$. Catalysts particle sizes were in the 0.40–0.60 mm range.

In the case of single-bed studies, a catalyst amount of 0.5 g was loaded into the reactor diluted with silicon carbide (SiC). Alternatively,

for combined bed experiments, each catalyst (0.2–0.5 g, diluted with SiC) was incorporated in two different subsequent catalytic beds, maintaining the total bed volume in all cases for a proper comparison. For catalytic results, a reaction time of 90 min was considered for each point. It must be noted that no space is considered between catalysts in the double bed configuration.

The effluent stream was bubbled through a condenser at ca. 0 °C. The remaining gaseous stream containing carbon oxides and oxygen was analyzed with an online gas chromatograph equipped with: (i) molecular sieves 5 Å (3 m); and (ii) Porapak Q (3 m). The condensed aqueous solution containing all the reaction products and the unconverted glycerol was analyzed by GC with a Varian 3900 chromatograph equipped with a 100 % dimethylpolysiloxane capillary column (100 m × 0.25 mm × 0.5 μm) [36].

3. Results and discussion

3.1. Physicochemical characteristics of catalysts

Most relevant physicochemical characteristics of samples studied here, W-based HTB and MoV-based M1 catalysts, are shown in Table 1.

Fig. 1 shows, separately, the XRD patterns and NH_3-TPD analyses of heat-treated catalysts. Then, in the case of W-based catalysts (Fig. 1A), it can be seen that the HTB, hexagonal bronze structure (*h*-WO_x, JCPDS: 33–1387), is achieved for both ***h*-WVO** and ***h*-WNbO** catalysts, with main diffraction peaks at 2θ= 14.0, 23.2, 28.1 and 36.9° [25,26], showing as reference the XRD pattern of pure *h*-WO_3 oxide (***h*-WO_x** sample). Moreover, for M1 phase-containing catalysts (i.e., **MoVO**, **MoVTeO** and **MoVTeNbO** samples, Fig. 1B), diffraction peaks at 2θ= 6.7, 7.9, 9.0, 10.8, 23.0 and 27.3° confirm the presence of the orthorhombic $(TeO)_2M_{20}O_{56}$, the so-called M1 phase (JCPDS: 18–582) [35]. In addition, it can be observed a different relative intensity of the main diffraction peaks (Fig. 1B), which corresponds to a different shape of the crystals, as reported in Figure S1, with crystals presenting needle-like morphology that transforms into rod-like shape in the case of the **MoVTeNbO** catalyst. Nevertheless, HTB oxides (i.e., ***h*-WO_x**, ***h*-WVO** and ***h*-WNbO** samples) present a similar rod-like structure, with the partial substitution of Nb^{5+} for W^{6+}/W^{5+} cations resulting into a decrease of the particle size [37].

Conversely, the acid properties of the different catalysts were studied by NH_3-TPD-MS, and experimental results are displayed in Figs. 1C and 1D. In this sense, two different trends can be observed depending on the composition of the catalyst. In one hand, for W-based catalysts (Fig. 1C), the incorporation of niobium or vanadium (***h*-WNbO** and ***h*-WVO** samples) leads to a decrease in the strength of the acid sites of both catalysts as the temperature maximum is shifted to lower temperature compared to that of pure *h*-WO_3 in the two cases. Furthermore, it is also observed that the incorporation of vanadium into the structure of the HTB oxide results in a further decrease of the strength of the acid sites, however, this catalyst is expected to present also redox activity. On the other hand, results for M1-presenting catalysts shown in Fig. 1D demonstrate that these catalysts should mainly present redox activity, with main desorption signal observed at ca. 175 °C, only observing some kind of acid strength behavior in the case of bimetallic **MoVO** catalyst, as reported previously [35].

Table 1
Physicochemical characteristics of W-based and Mo-based catalysts.

Sample	Atomic composition (%)		Crystaline phase (XRD)	S_{BET}[a] (m^2 g^{-1})	Acid sites[b] (TPD-NH_3)
	EDS	XPS			
***h*-WO_x**	100/0/0	100/0/0	HTB	31	256.3
***h*-WNbO**	75/0/25	73/0/27	HTB	98	1152.1
***h*-WVO**	82/18/0	91/9/0	HTB	22	1176.1
MoVO	73/27/0/0	85/15/0/0	M1	35	151.8
MoVTeO	65/30/5/0	82/14/4/0	M1	8	16.1
MoVTeNbO	58/13/15/13	55/8/22/15	M1	5	21.5

[a] Surface area, S_{BET}, calculated from N_2 adsorption isotherms by applying the BET method

[b] density of acid sites, determined by TPD-NH_3 experiments and expressed in $\mu mol_{NH3}\ g_{cat}^{-1}$

Then, to study the different redox properties of the catalysts, XPS analyses were conducted, and results are plotted in Fig. 2A and Table 1. More detailed results of the surface composition of these samples are presented in Table S1, observing that the main differences among catalysts are seen in the vanadium *2p* core level signal. Accordingly, as it has been suggested, the control of the V^{4+}/V^{5+} ratio on the surface of a catalyst is a pivotal fact to obtain good catalysts for partial oxidation reactions [35]. So, in Fig. 2A it is observed a tendency in the V^{4+}/V^{5+} ratio depending on the chemical composition of the catalyst, seeing that all M1-presenting catalysts show a majority abundance of V^{4+} species. On the contrary, in the case of the ***h*-WVO** catalyst, similar amount of V^{4+} and V^{5+} species can be deconvoluted, indicating a higher ability of this sample for total oxidation reactions.

These results agree with the fact that the dehydration of glycerol to acrolein should happen over Brønsted acid catalysts (this is the case of W-based samples [25,26,37]), while oxidation of acrolein to acrylic acid is rather driven by redox catalysts with low activity to deep oxidation reactions [25,36], as observed in M1 catalysts with a higher proportion of reduced V^{4+} species.

Moreover, in Fig. 2B is plotted the TPR-H_2 patterns for the two families of catalysts. There, two different trends are observed depending on the nature of the catalysts. For M1-phase catalysts, it can be seen that bimetallic **MoVO** catalyst shows higher bulk reducibility, with the first reduction maximum at ca. 470 °C, while both **MoVTeO** and **MoVTeNbO** samples present reduction maxima at ca. 500 °C, which corresponds to the reduction of V-O-Mo sites and agrees with the higher activity of the **MoVO** sample, since in this case the reduction starts at temperatures around 250 °C. Moreover, it is also observed for this catalyst that temperatures above 600 °C lead to the collapse of the structure, seen in Fig. 2 and also reported elsewhere [35], due to the absence of -Te-O-Te- chains along the hexagonal channels of the M1 structure. Conversely, in the case of HTB oxides, the first reduction maximum for the ***h*-WVO** catalyst appears at ca. 530 °C corresponding to surface W-O-V pairs, while bulk reduction occurs at temperatures above 600°C (ca. 725 °C, although not shown in the figure) [26]. However, in the case of ***h*-WO_x** and ***h*-WNbO** catalysts, there is no reduction of the W and Nb species.

In addition to this, since reduction of the surface of each catalyst varies and relates to the different catalytic activity, it is important to study the onset temperatures in the TPR-H_2 profiles. Then, in Fig. 2B onset temperatures are also represented (in blue). There, it can be seen that the **MoVO** sample is the catalyst with the reduction onset at the lowest temperature (ca. 250 °C), while both **MoVTeO** and **MoVTeNbO** catalysts present similar onset temperature, at ca. 300 °C. On the contrary, in the case of the ***h*-WVO** sample, reduction onset temperature rises to ca. 320 °C, in agreement with the lower global reducibility of W-based catalysts.

3.2. Catalytic results

Catalytic results for the transformation of glycerol into acrolein and/or acrylic acid in single or double bed configurations are shown in Tables 2 and 3, respectively.

Fig. 3 shows the catalytic results for tungsten-based catalysts at different reaction temperatures in a single catalytic bed configuration. It must be noted that the results shown in Fig. 3 correspond to a 100 % glycerol conversion regardless of the reaction temperature. Then, huge differences can be ascertained in the selectivity to the different desired products depending on the composition of the catalyst and the reaction

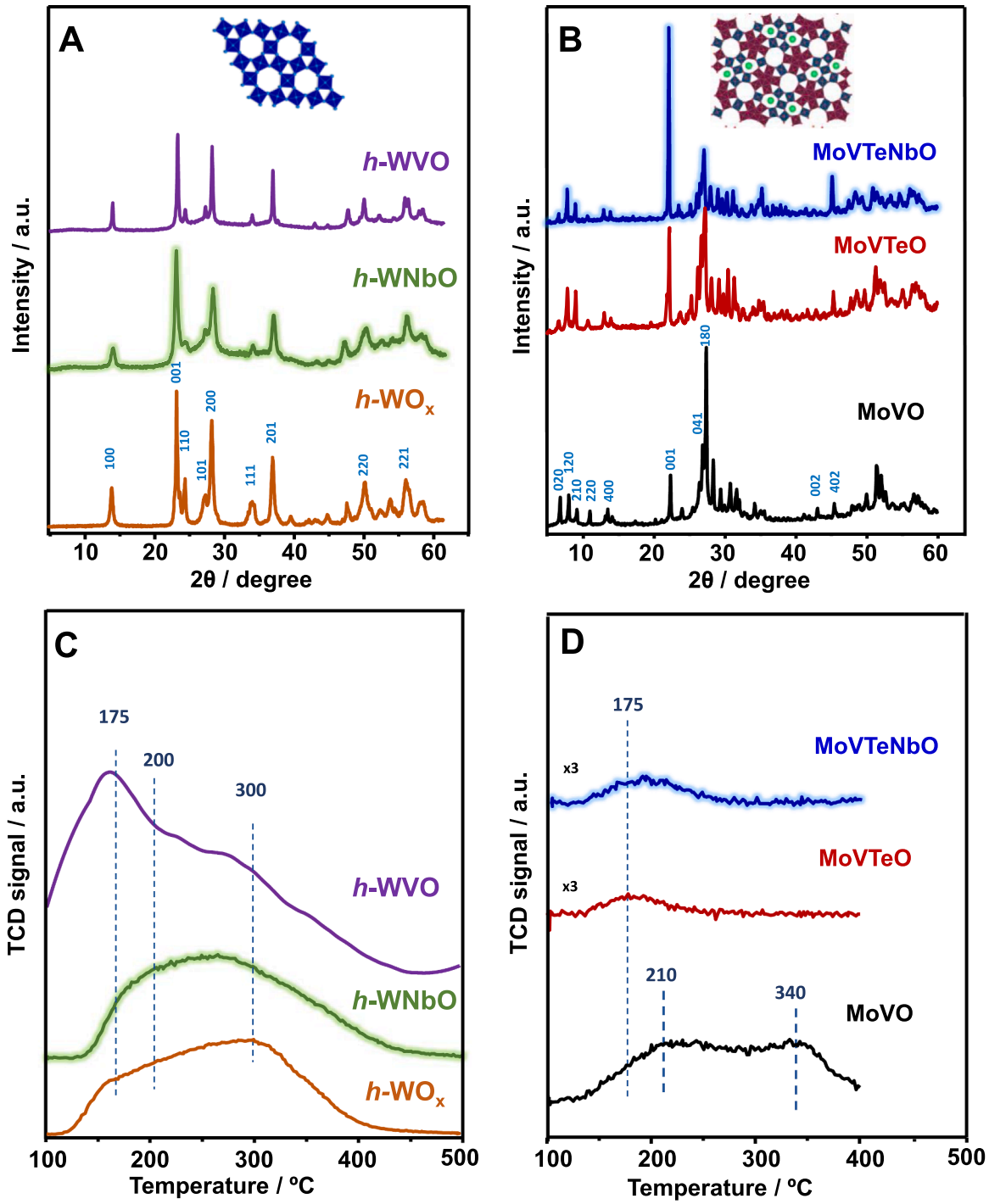

Fig. 1. XRD patterns (A, B) and NH_3-TPD analyses (C, D) of catalysts. HTB-type catalysts: ***h*-WO$_x$**; ***h*-WNbO**; ***h*-WVO.** M1-phase catalysts: **MoVO**; **MoVTeO** and **MoVTeNbO**.

temperature. Accordingly, mainly acid catalysts (i.e., samples ***h*-WO$_x$** and ***h*-WNbO**) display excellent results in terms of selectivity to acrolein, with relatively low CO_x formation. In this sense, both ***h*-WO$_x$** and ***h*-WNbO** catalysts exhibit a selectivity to acrolein of ca. 80 % at reaction temperatures lower than 340 °C (Figs. 3A and 3C, respectively). Moreover, the formation of both CO and CO_2 is lower than 20 % in selectivity for both catalysts, regardless of the reaction temperature (Figs. 3B and 3D, respectively), although showing an increasing tendency with the reaction temperature.

On the contrary, catalyst that presents also redox activity, this is ***h*-WVO** sample, perform poorly in the formation of acrolein. Nevertheless, ***h*-WVO** catalyst is able to form acrylic acid in one step, with moderate selectivity results (ca. 25 % selectivity to acrylic acid at 290 °C, Fig. 3E). In any case, by increasing the reaction temperature the formation of CO_x over this catalyst is highly favored (up to 50 % selectivity to CO at 390 °C of reaction temperature, Fig. 3F). In the case of M1-based catalysts, it is only observed the formation of CO_x in the **MoVO** sample, with a little formation of acrylic acid. In the case of the **MoVTeNbO** catalyst, acrylic acid is the main oxygenated product (ca. 15 %), with the subtle formation of both acrolein and acetic acid in agreement with its very low concentration of both Lewis and Brønsted acid sites. In any case, the V-containing catalysts (i.e., ***h*-WVO**, **MoVO**, and **MoVTeNbO**) show a

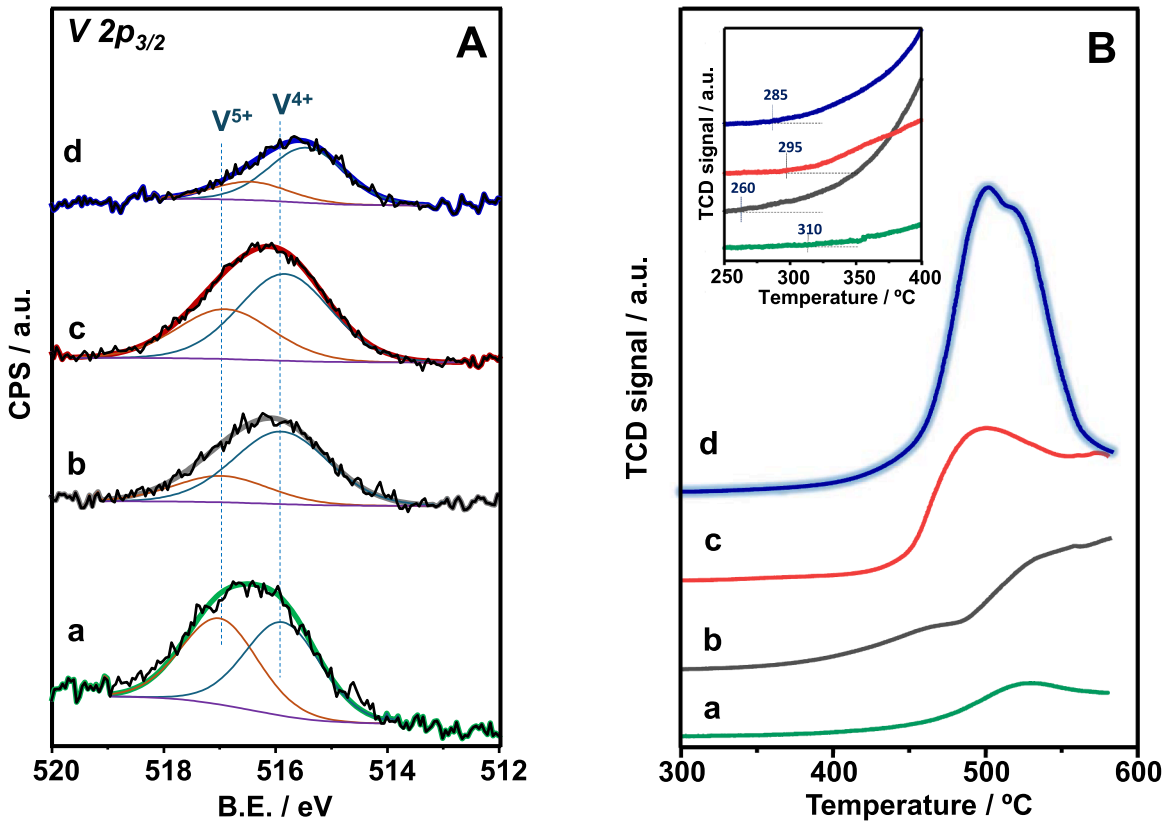

Fig. 2. XPS of V $2p_{3/2}$ peaks (A) and TPR-H_2 results (B) of V-containing catalysts: a) ***h*-WVO**; b) **MoVO**; c) **MoVTeO**; and, d) **MoVTeNbO**.

Table 2
Catalytic results during the glycerol transformation into acrolein and acrylic acid of W-based and Mo-based catalysts in single bed configuration.

Sample	Selectivity (%)[a]						
	Acrolein	Acrylic Acid	Acetaldehyde	Acetic Acid	CO	CO_2	Heavy Comp.
***h*-WO_x**	77.8	0.1	4.6	0.6	6.6	4.4	6.0
***h*-WNbO**	79.5	0.6	2.9	0.6	6.9	4.9	4.8
***h*-WVO**	13.6	19.7	1.2	5.1	23.7	19.0	17.7
MoVO	1.2	7.0	0.2	8.3	46.9	24.5	11.8
MoVTeNbO	4.6	14.8	0.6	3.4	37.8	21.1	17.3

[a] Selectivity data taken at 320 °C reaction temperature, 3 h of reaction time and full glycerol conversion.

Table 3
Catalytic results during the glycerol transformation intro acrolein and acrylic acid of double bed configuration catalysts.

Sample(double bled)	Selectivity (%)[a]						
	Acrolein	Acrylic Acid	Acetaldehyde	Acetic Acid	CO	CO_2	Heavy Comp.
***h*-WNbO + MoVO**	13.4	48.9	4.6	4.3	9.1	6.5	17.1
***h*-WNbO + MoVTeO**	7.3	56.4	0.5	4.2	12.9	8.1	11.1
***h*-WNbO + MoVTeNbO**	12.3	61.6	0.8	4.1	9.5	6.5	5.2

[a] Selectivity data taken at 320 °C reaction temperature, three hours of reaction time and full glycerol conversion.

notable formation of non-analyzable heavy compounds, in the 12–18 % range depending on the sample, along with the preferential formation of CO over CO_2.

Therefore, provided that in one single step the formation of acrylic acid is not sufficiently accomplished, a double catalytic bed configuration is considered. In this sense, a first Brønsted-based catalytic bed is assumed in order to maximize the transformation of glycerol into acrolein, employing the ***h*-WNbO** sample as said first catalytic bed, followed by a subsequent oxidizing catalytic bed (i.e., M1-based catalysts).

Accordingly, in Fig. 4 and Table 3, results for the one pot transformation of glycerol into acrylic acid and/or acrolein, in a double

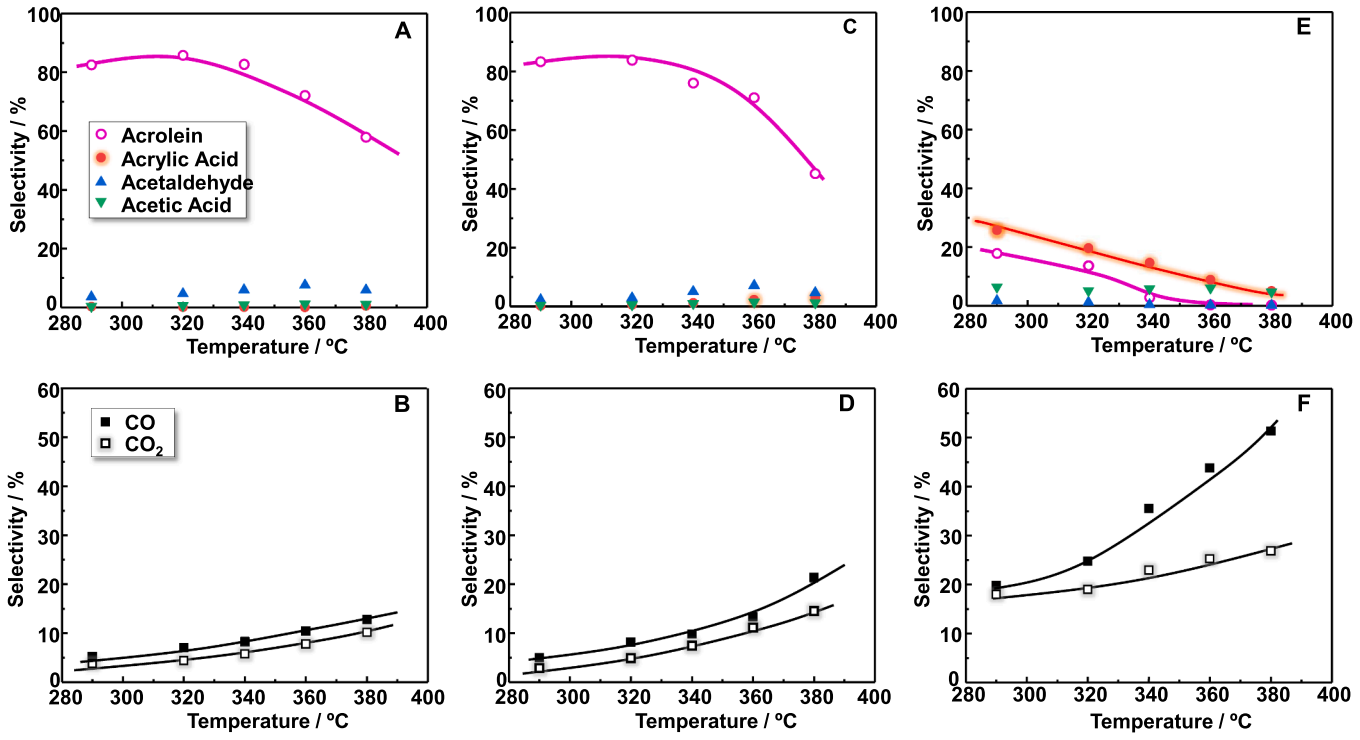

Fig. 3. Selectivity to the main reaction products in the single bed configuration oxidation of glycerol of ***h*-WO$_x$** (A and B), ***h*-WNbO** (C and D) and ***h*-WVO** (E and F) catalysts. Products: acrolein (red), acrylic acid (pink), acetaldehyde (blue) and acetic acid (green). Conversely, deep oxidation products are represented as CO (■) and CO_2 (□).

catalytic bed configuration (Fig. 4D), are shown. For these experiments, a reaction temperature of 320 °C is fixed since the best results in one bed configuration (Fig. 3) were obtained at said temperature. According to the results in Fig. 4, it can then be seen a relatively higher selectivity towards acrylic acid, although the final selectivity to acrylic acid is strongly influenced by the composition of the catalyst in the second catalytic bed.

Fig. 4A shows the stability of the double catalytic bed configuration by employing the **MoVO** sample as the oxidizing bed. In that figure, the selectivity to acrylic acid varies in the 40–50 % range in eight hours of reaction, without showing a decrease in selectivity.

Furthermore, selectivity to acrolein fluctuates in the 10–20 % range. In a similar way, Figs. 4B and 4C show the selectivity to acrylic acid or acrolein using **MoVTeO** and **MoVTeNbO** catalysts as subsequent oxidizing beds, respectively. Interestingly, selectivity to acrylic acid seems to increase with the chemical composition of this M1 phase, this is, selectivity to acrylic acid increases as follows: **MoVO** < **MoVTeO** < **MoVTeNbO**. Thus, a maximum selectivity of ca. 65 % to acrylic acid can be obtained by using a ***h*-WNbO** followed by **MoVTeNbO** configuration (Fig. 4C).

On top of this, it is also observed from these reactions (see Table 3) that the formation of heavy compounds also decreases with the increase in the selectivity to acrylic acid. Then, it is suggested that the formation of these heavy compounds corresponds to the reaction between the organic molecules of the reaction to form condensation products.

3.3. In situ FTIR spectroscopy study with acrolein

The interaction and surface reactivity of acrolein adsorbed on the catalyst surface has been studied by IR spectroscopy (details in experimental section) in order to correlate with the above reported catalytic data. Moreover, specific assignation of the IR bands is presented in Table S2, Supporting Information. Then, as reflected in Fig. 5, different reactivity patterns are observed on the different samples. Thus, practically no acrolein adsorption is observed in the **MoVTeNbO** sample (Fig. 5A), just small bands at 1545, 1605 and 1721 cm^{-1}, related to the lower oxidation of both acrolein and acrylic acid into higher carbon number oxygenate compounds. Conversely, in the case of the **MoVTeO** catalyst (Fig. 5B), a series of IR bands at 1670, 1650, 1628 and 1609 cm^{-1} together with bands at 1522, 1430, 1360 and 1271 cm^{-1} are formed at 25°C after acrolein adsorption. The bands at 1670–1650 cm^{-1}, and 1628 cm^{-1} can be ascribed to the respective υ (C═O) and υ (C═C) frequency of acrolein interacting with surface Lewis sites such as V^{5+}/V^{4+} [36,38–41]. The IR bands at 1522, 1430, 1360 and 1271 cm^{-1} are assigned to adsorbed acetate species [42,43], probably precursor of CO_2 formation. The band at 1609 cm^{-1} may correspond to the stretching vibration of -COOH [44], or C-O-C vibration of ether-like species. Finally, the IR band at 1709 cm^{-1} may correspond to acetic acid. Moreover, by increasing the reaction temperature to 100 and 150°C, the intensity of all the IR bands decreases and finally they practically disappear at 200 and 250 °C. This loss of the IR signal is due to the desorption of the different compounds to the gas phase, as confirmed from reabsorption spectra (see dotted line in Fig. 5B), which is obtained by cooling down to room temperature the IR cell. Furthermore, on the **MoVO** sample, a similar trend as in the **MoVTeO** sample is observed at 25 °C (Fig. 5C), with acrolein interacting with Lewis sites (1666 and 1626 cm^{-1}), and the presence of adsorbed acetate species (1525, 1417, 1365 and 1274 cm^{-1}) precursor of CO_2 and acetic acid (1705 cm^{-1}). At increasing temperatures, all bands decrease drastically in intensity due to gas phase desorption, as observed from the read-sorption IR spectra (see dotted line already mentioned). Finally, on the ***h*-WVO** catalyst (Fig. 5D), a different behavior is observed. Interestingly, it is evidenced a higher interaction strength of surface adsorbed acrolein (1686, 1650 and 1620 cm^{-1}), being stable up to 320 °C (i.e., reaction temperature employed in the catalytic test). In this case, at increasing temperature of 250 °C, the formation of both acrylic acid (1725 cm^{-1}) and surface cyclic species is also observed (1780 cm^{-1}). On the contrary, the amount of surface acetate species (bands at 1426 and, not shown in here, 1362 cm^{-1}) is markedly lower, correlating with the lower CO_2 formation in the single bed catalytic studies when compared to

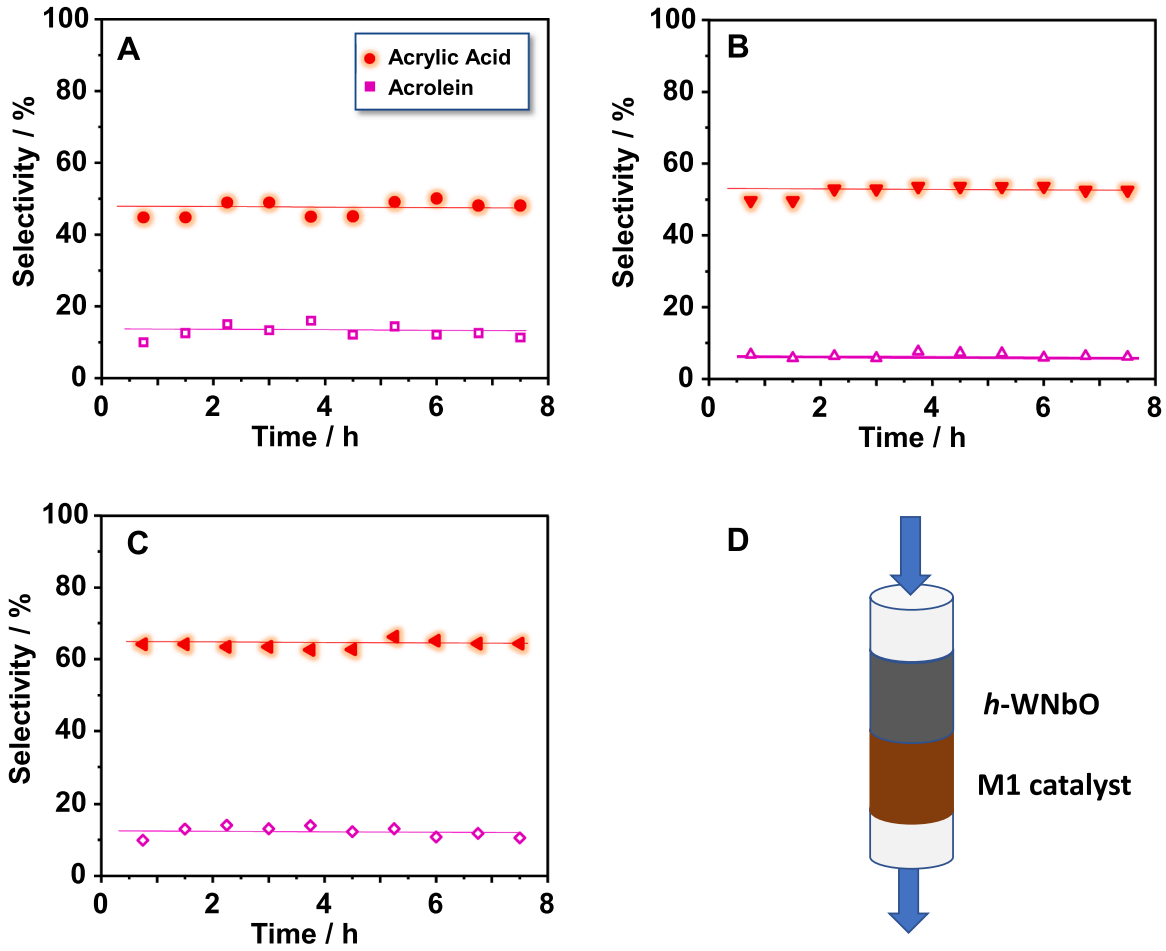

Fig. 4. Stability test for glycerol transformation into acrylic acid and/or acrolein in a double bed configuration: A) ***h*-WNbO + MoVO** (M1); B) ***h*-WNbO + MoVTeO** (M1); and C) ***h*-WNbO + MoVTeNbO** (M1). D) Configuration of a double bed catalytic systems.

M1-based catalysts. Nonetheless, the higher surface interaction of acrolein with the ***h*-WVO** catalyst allows further oxygenation to acrylic acid but also to carbon oxides [36], in agreement to catalytic results in single catalytic bed configuration. In contrast, for M1-based samples, **MoVO**, **MoVTeO** and **MoVTeNbO**, the interaction of acrolein on the surface is lower, favoring gas phase desorption and a lower influence of consecutive reactions, being a reason of the good acrolein oxidation performance when employed as second catalytic bed in the direct glycerol to acrylic acid transformation, already reported [30–34]. Furthermore, the different reactivity of surface oxygen species may result in the formation of acetate-like species depending on the catalyst, being higher in the **MoVO** and **MoVTeNbO** samples than in the ***h*-WVO** sample, leading to a higher CO_2 formation in the former. In line with this, the formation of a certain amount of acetic acid is also observed in the **MoVO**, **MoVTeO** and **MoVTeNbO** catalysts in the double bed configuration (see Table 3).

Finally, although it is well-known that the catalytic behavior of M1-containing oxides strongly depends on their chemical composition, previously reported for the partial for the partial propane amm(oxidation) to acrylic acid or acrylonitrile [6,45–47] or for the oxidative dehydrogenation of ethane to ethylene [35,47,48], it must be noted that these spectroscopic results also correlate with the catalytic behavior showed in this paper.

Then, MoVO materials have been proposed as very active and selective catalysts for the partial oxidation of acrolein to acrylic acid [49], nevertheless, these results only concern oxidation of pure acrolein whereas, in our case, the presence of small amounts of by-products rather than CO and CO_2, and formed during the dehydration of glycerol to acrolein, could modify the catalytic performance of M1-based catalysts.

4. Conclusions

In the present article, the one-pot transformation of glycerol into acrylic acid has been studied by following two different approaches. On the one hand, single catalytic bed configuration employing bronze-type tungsten oxide catalysts (presenting the well-known hexagonal structure, HTB) or orthorhombic molybdenum based mixed metal oxides (so-called M1 structure). On the other hand, the use of a double catalytic bed configuration consisting of a first acid catalyst (***h*-WNbO**) followed by an oxidizing M1-based catalyst (**MoVO**, **MoVTeO** or **MoVTeNbO**).

Then, results in a single catalytic bed configuration demonstrated that an acid catalyst is required to firstly dehydrate the glycerol into acrolein, in particular, catalysts that mainly present Brønsted acid sites (i.e., ***h*-WO_x** and ***h*-WNbO** samples). Conversely, samples that consist of redox behavior, namely the ones that contain vanadium species in their structure (***h*-WVO**, **MoVO** and **MoVTeNbO** catalysts) tend to deeply oxidize the glycerol molecule into either heavy oxygenated compounds or carbon oxides (CO mainly, but also CO_2).

Therefore, to overcome the problems observed using only one catalyst, a subsequent double bed configuration in a unique reactor was studied. In this case, since acrolein is a mandatory intermediate formed during the reaction mechanism [36], the first catalytic bed consisted of a pure acid catalyst (this is ***h*-WNbO** sample), that proved to yield ca. 80 % acrolein from glycerol under the used reaction conditions (320–350 °C). Then, provided that the further oxidation of acrolein into acrylic acid is

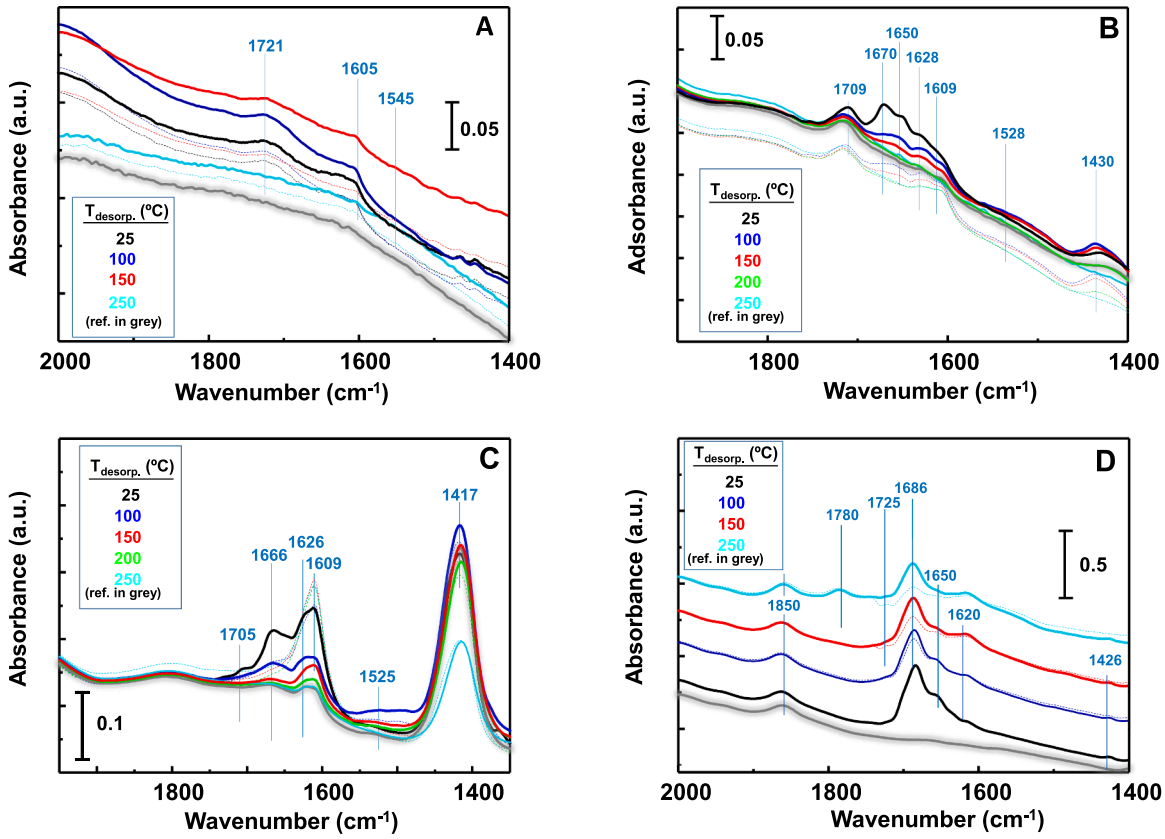

Fig. 5. IR spectra of acrolein adsorption on **MoVTeNbO** (A) **MoVTeO** (B), **MoVO** (C) and ***h*-WVO** (D) samples, and their evolution at increasing temperatures. Doted lines correspond to gas phase readsorption spectra. More details in experimental section.

driven by redox mechanisms [36,38,39,44], M1-based catalysts were used in a second subsequent independent catalytic bed. Results in this configuration improved up to 40–65 % acrylic acid yield, depending on the chemical composition of the M1 phase catalyst, showing how the best results (up to 65 % yield directly from glycerol) were obtained with the ***h*-WNbO** + M1-**MoVTeNbO** system. Nevertheless, if we consider the acrylic acid yield with respect to acrolein, catalytic results indicate an acrylic acid yield up to ca. 81 % (acrolein-based) over this system.

Accordingly, an *in situ* IR study of co-adsorbed acrolein and O_2 over the oxidizing catalyst revealed that the surface of pure redox materials such as the M1-phase containing catalysts interact softer with the acrolein, rather than the ***h*-WVO** catalyst, that also present acid sites but in a far lesser extent compared to the rest of the HTB catalysts (i.e., ***h*-WO_x** and ***h*-WNbO**), explaining the better catalytic results of the former ones. In addition to this, both catalytic and spectroscopic differences among the **MoVO**, **MoVTeO** and **MoVTeNbO** catalysts are explained on the basis of the greater of lesser strength of adsorption of the acrolein on the surface of the catalyst, with the consequent formation of oxygenated heavy compounds, as observed in Table 3, since the distribution of the rest of the products remain intrinsically the same regardless of the chemical composition of the M1 phase catalyst.

CRediT authorship contribution statement

Agustín de Arriba: Writing – review & editing, Writing – original draft, Validation, Investigation. **Daniel Delgado:** Writing – review & editing, Writing – original draft, Investigation. **Patricia Concepción:** Writing – review & editing, Writing – original draft, Validation, Supervision, Conceptualization. **José M. López Nieto:** Writing – review & editing, Writing – original draft, Supervision, Funding acquisition, Conceptualization.

Declaration of Competing Interest

The authors declare that they have no known competing financial interests or personal relationships that could have appeared to influence the work reported in this paper.

Data Availability

Data will be made available on request.

Acknowledgement

The funding received for this study from the Spanish Ministry of Science and Innovation, PID2021-126235OB-C31 funded by MCIN/AEI/10.13039/501100011033 and FEDER funds, and project TED2021-130756B-C32 funded by MCIN/AEI/10.13039/501100011033 and by "ERDF A way of making Europe" by the European Union NextGenerationEU/PRTR, is acknowledged.

This Special Issue is dedicated to honor the 10th International Symposium on Group V (IV and VI) Elements, a gathering of international researchers, industry, young researchers, and students to help shape the vision of the future for these elements.

Appendix A. Supporting information

Supplementary data associated with this article can be found in the online version at doi:10.1016/j.cattod.2024.114965.

References

[1] T. Ohara, T. Sato, N. Shimizu, G. Prescher, H. Schwind, O. Weiberg, K. Marten, H. Greim, Acrylic acid and derivatives, in: B. Elvers (Ed.), Ullmann's Encyclopedia of Industrial Chemistry, Wiley-VCH Verlag, 2003.

[2] ⟨https://www.statista.com/statistics/1245262/acrylic-acid-market-volume-worldwide/#:~:text=In%202022%2C%20the%20market%20volume,worldwide%20in%20the%20year%202030⟩.

[3] K. Weissermel, H.-J. Arpe. Industrial Organic Chemistry, Wiley-VCH, New York, 2003, p. 2314.

[4] L.H. Vieira, A. Lopez-Castillo, C.W. Jones, L. Martins, Exploring the multifunctionality and accessibility of vanadosilicates to produce acrylic acid in one-pot glycerol oxydehydration, Appl. Catal. A-Gen. 602 (2020) 117687.

[5] R.K. Grasselli, J.D. Burrington, D.J. Buttrey, P. DeSanto Jr., G. Cl, Lugmair, A.F. Volpe Jr., T. Weingand, Multifunctionality of active centers in (amm)oxidation catalysts: from Bi–Mo–Ox to Mo–V–Nb–(Te;Sb)–Ox, Top. Catal. 23 (2003) 5–22.

[6] J.M. Oliver, J.M. López Nieto, P. Botella, Selective oxidation and ammoxidation of propane on a Mo-V-Te-Nb-O mixed metal oxide catalyst: a comparative study, Catal. Today 96 (2004) 241–249.

[7] W. Ueda, D. Vitry, T. Katou, Structural organization of catalytic functions in Mo-based oxides for propane selective oxidation, Catal. Today 96 (2004) 235–240.

[8] M. Hävecker, S. Wrabetz, J. Kröhnert, L. Csepei, R.N. d'Alnoncourt, Y.V. Kolen'ko, F. Girgsdies, R. Schlögl, A. Trunschke, Surface chemistry of phase-pure M1 MoVTeNb oxide during operation in selective oxidation of propane to acrylic acid, J. Catal. 285 (2012) 48–60.

[9] H.-G. Lintz, S.P. Müller, The partial oxidation of propane on mixed metal oxides-A short overview, Appl. Catal. A- Gen. 357 (2009) 178–183.

[10] G. Hayes, M. Laurel, D. MacKinnon, T. Zhao, H.A. Houck, C.R. Becer, Polymers without petrochemicals: sustainable routes to conventional monomers, Chem. Rev. 123 (2023) 2609–2734.

[11] M. Onn, M.J. Jalil, N.I.S.M. Yusoff, E.B. Edward, M.U. Wahit, A comprehensive review on chemical route to convert waste cooking oils to renewable polymeric materials, Ind. Crop. Prod. 211 (2024) 118194.

[12] K. Avasthi, A. Bohre, M. Grilc, B. Likozar, B. Saha, Advances in catalytic production processes of biomass-derived vinyl monomers, Catal. Sci. Technol. 10 (2020) 5411–5437.

[13] X. Jin, K. Meng, G. Zhang, M. Liu, Y. Song, Z. Song, C. Yang, Interfacial catalysts for sustainable chemistry: advances on atom and energy efficient glycerol conversion to acrylic acid, Green. Chem. 23 (2021) 51–76.

[14] U.C. Abubakar, Y. Bansod, L. Forster, V. Spallina, C. D'Agostino, Conversion of glycerol to acrylic acid: a review of strategies, recent developments and prospects, React, Chem. Eng. 8 (2023) 1819–1838.

[15] D. Sun, Y. Yamada, S. Sato, W. Ueda, Glycerol as a potential renewable raw material for acrylic acid production, Green. Chem. 19 (2017) 3186–3213.

[16] (a) M.Y. Ahmad, N.I. Basir, A.Z. Abdullah, A review on one-pot synthesis of acrylic acid from glycerol on bi-functional catalysts, J. Ind. Eng. Chem. 93 (2021) 216–227;
(b) A. Abdullah, A.Z. Abdullah, M. Ahmed, P.U. Okoye, M. Shahadat, A review on bi/multifunctional catalytic oxydehydration of bioglycerol to acrylic acid: Catalyst type, kinetics, and reaction mechanism, Can. J. Chem. Eng. 100 (2022) 2956–2985.

[17] Sh.T. Wu, Q.M. She, R. Tesser, M. Di Serio, Ch.H. Zhou, Catalytic glycerol dehydration-oxidation to acrylic acid, Catal. Rev. Sci. Eng. 62 (2020) 481–523.

[18] C.B. Rasrendra, N.T.U. Culsum, A. Rafiani, G.T.M. Kadja, Glycerol valorization for the generation of acrylic acid via oxidehydration over nanoporous catalyst: Current status and the way forward, Bioresour. Technol. Rep. 23 (2023) 101533.

[19] X. Li, Y. Zhang, Oxidative dehydration of glycerol to acrylic acid over vanadium-substituted cesium salts of keggin-type heteropolyacids, ACS Catal. 6 (2016) 2785–2791.

[20] A. Abdullah, M. Ahmed, A.Z. Abdullah, Selective production of acrylic acid from glycerol through a single-stage gas phase catalytic oxydehydration over Vanadium-incorporated Zeolite Beta Catalysts, Waste Biomass. Valori. 15 (2024) 163–175.

[21] J. Deleplanque, J.-L. Dubois, J.-F. Devaux, W. Ueda, Catal. Today 157 (2010) 351–358.

[22] L.G. Possato, W.H. Cassinelli, C.I. Meyer, T. Garetto, S.H. Pulcinelli, C.V. Santilli, L. Martins, Thermal treatments of precursors of molybdenum and vanadium oxides and the formed $Mo_xV_yO_z$ phases active in the oxydehydration of glycerol, Appl. Catal. A- Gen. 532 (2017) 1–11.

[23] L.F. Rasteiro, L.H. Vieira, C.V. Santilli, L. Martins, Surfactant-assisted synthesis of Mo–V mixed oxide catalysts for upgraded one-step conversion of glycerol to acrylic acid, RSC Adv. 8 (2018) 11975–11982.

[24] L. Shen, H. Yin, A. Wang, X. Lu, Ch Zhang, Gas phase oxidehydration of glycerol to acrylic acid over Mo/V and W/V oxide catalysts, Chem. Eng. J. 244 (2014) 168–177.

[25] M.D. Soriano, ungsten-vanadium mixed oxides for the oxidehydration of glycerol into acrylic acid, Green. Chem. 13 (2011) 2954–2962.

[26] A. Chieregato, F. Basile, P. Concepción, S. Guidetti, G. Liosi, M.D. Soriano, C. Trevisanut, F. Cavani, J.M. López Nieto, Glycerol oxidehydration into acrolein and acrylic acid over W–V–Nb–O bronzes with hexagonal structure, Catal. Today 197 (2012) 58–65.

[27] K. Omata, K. Matsumoto, T. Murayama, W. Ueda, Direct oxidative transformation of glycerol to acrylic acid over Nb-based complex metal oxide catalysts, Catal. Today 259 (2016) 205–212.

[28] Y.S. Yun, K.R. Lee, H. Park, T.Y. Kim, D. Yun, J.W. Han, J. Yi, Rational design of a bifunctional catalyst for the oxydehydration of glycerol: a combined theoretical and experimental study, ACS Catal. 5 (2015) 82–94.

[29] A. Chieregato, M.D. Soriano, E. García-González, G. Puglia, F. Basile, P. Concepción, C. Bandinelli, J.M. López Nieto, F. Cavani, Multielement crystalline and pseudocrystalline oxides as efficient catalysts for the direct transformation of glycerol into acrylic acid, ChemSusChem 8 (2015) 398–406.

[30] J.L. Dubois, C. Duquenne, W. Hölderich, Method for Producing Acrylic Acid from Glycerol. US 7,910,771 B2 (2011); assigned to Arkema France.

[31] A. Witsuthammakul, T. Sooknoi, Direct conversion of glycerol to acrylic acid via integrated dehydration-oxidation bed system, Appl. Catal. A-Gen. 413– 414 (2012) 109–116.

[32] Y.S. Yun, K.R. Lee, H. Park, T.Y. Kim, D. Yun, J.W. Han, J. Yi, Rational design of a bifunctional catalyst for the oxydehydration of glycerol: a combined theoretical and experimental study, ACS Catal. 5 (2015) 82–94.

[33] L. Liu, B. Wang, Y. Du, Z. Zhong, A. Borgna, Bifunctional $Mo_3VO_x/H_4SiW_{12}O_{40}/Al_2O_3$ catalysts for one-step conversion of glycerol to acrylic acid: Catalyst structural evolution and reaction pathways, Appl. Catal. B-Environm. 174–175 (2015) 1–12.

[34] R. Liu, T. Wang, D. Cai, Y. Jin, Highly efficient production of acrylic acid by sequential dehydration and oxidation of glycerol, Ind. Eng. Chem. Res. 53 (2014) 8667–8674.

[35] A. de Arriba, G. Sánchez, R. Sánchez-Tovar, P. Concepción, R. Fernández-Domene, B. Solsona, Jose M. López Nieto, On the selectivity to ethylene during ethane ODH over M1-based catalysts. A surface and electrochemical study, Catal. Today 418 (2023) 114122.

[36] A. Chieregato, C. Bandinelli, P. Concepción, M.D. Soriano, F. Puzzo, F. Basile, F. Cavani, J.M. López Nieto, Structure–reactivity correlations in vanadium-containing catalysts for one-pot glycerol oxidehydration to acrylic acid, ChemSusChem 10 (2017) 234–244.

[37] D. Delgado, P. Concepción, A. Trunschke, J.M. López, Nieto, Tungsten–niobium oxide bronzes: a bulk and surface structural study, Dalton Trans. 49 (2020) 13282–13293.

[38] T.V. Andrushkevich, G.Ya Popova, Mechanism of heterogeneous oxidation of acrolein to acrylic acid, Russ. Chem. Rev. 60 (1991) 1023–1034.

[39] J. Tichý, Oxidation of acrolein to acrylic acid over vanadium-molybdenum oxide catalysts, Appl. Catal. A-Gen. 157 (1997) 363–385.

[40] T.V. Andrushkevich, Heterogeneous catalytic oxidation of acrolein to acrylic acid: mechanism and catalysts, Catal. Rev. -Sci. Eng. 35 (1993) 213–259.

[41] J.M. López Nieto, B. Solsona, P. Concepción, F. Ivars, A. Dejoz, M.I. Vázquez, Reaction products and pathways in the selective oxidation of C_2-C_4 alkanes on MoVTeNb mixed oxide catalysts, Catal. Today 157 (2010) 291–296.

[42] D. Shee, G. Deo, Adsorption and ODH reaction of alkane on sol–gel synthesized TiO_2–WO_3 supported vanadium oxide catalysts: In situ DRIFT and structure–reactivity study, J. Mol. Catal. A-Chem. 308 (2009) 46–55.

[43] J. Ma, L. Duan, J. Lu, B. Lyu, D. Gao, X. Wu, Fabrication of modified hydrogenated castor oil/GPTMS-ZnO composites and effect on UV resistance of leather, Sci, Report 7 (2017) 3742.

[44] K.I. Hadjiivanov, D.A. Panayotov, M.Y. Mihaylov, E.Z. Ivanova, K.K. Chakarova, S. M. Andonova, N.L. Drenchev, Power of infrared and raman spectroscopies to characterize metal-organic frameworks and investigate their interaction with guest molecules, Chem. Rev. 121 (2021) 1286–1424.

[45] W. Ueda, K. Oshihara, D. Vitry, T. Hisano, Y. Kayashima, Hydrothermal synthesis of Mo-based oxide catalysts and selective oxidation of alkanes, Catal. Surv. Jpn 6 (2002) 33–44.

[46] W. Ueda, D. Vitry, T. Katou, Crystalline Mo–V–O based complex oxides as selective oxidation catalysts of propane, Catal. Today 99 (2005) 43–49.

[47] P. Concepción, S. Hernández, J.M. López Nieto, On the nature of active sites in MoVTeO and MoVTeNbO catalysts: the influence of catalyst activation temperature, Appl. Catal. A-Gen. 391 (2011) 92–101.

[48] P. Botella, A. Dejoz, M.C. Abello, M.I. Vázquez, L. Arrúa, J.M. López, Nieto, Selective oxidation of ethane: developing an orthorhombic phase in Mo-V-X (X = Nb, Sb, Te) mixed oxides, Catal. Today 142 (2009) 273–277.

[49] S. Ishikawa, Y. Yamada, N. Kashio, N. Noda, K. Shimoda, M. Hayashi, T. Murayama, W. Ueda, True catalytically active structure in Mo-V-based mixed oxide catalysts for selective oxidation of acrolein, ACS Catal. 11 (2021) 10294–10307.